

# 1 Reconstruction of a daily gridded snow water equivalent product for 2 the land region above 45° N based on a ridge regression machine 3 learning approach

4 Donghang Shao<sup>1,2</sup>, Hongyi Li<sup>1,2</sup>, Jian Wang<sup>1,2</sup>, Xiaohua Hao<sup>1,2</sup>, Tao Che<sup>1,2</sup> and Wenzheng Ji<sup>1,2,3</sup>

5 <sup>1</sup>Northwest Institute of Eco-Environment and Resources, Chinese Academy of Sciences, Lanzhou, 730000, China

6 <sup>2</sup>Heihe Remote Sensing Experimental Research Station, Key Laboratory of Remote Sensing of Gansu Province, Chinese  
7 Academy of Sciences, Lanzhou, 730000, China

8 <sup>3</sup>University of Chinese Academy of Sciences, Beijing, 100049, China

9 *Correspondence to:* Hongyi Li (lihongyi@lzb.ac.cn)

10 **Abstract.** The snow water equivalent (SWE) is an important parameter of surface hydrological and climate systems, and it  
11 has a profound impact on Arctic amplification and climate change. However, there are great differences among existing SWE  
12 products. In the land region above 45° N, the existing SWE products are associated with a limited time span and limited  
13 spatial coverage, and the spatial resolution is coarse, which greatly limits the application of SWE data in cryosphere change  
14 and climate change studies. In this study, utilizing the ridge regression model (RRM) of a machine learning algorithm, we  
15 integrated various existing SWE products to generate a spatiotemporally seamless and high-precision RRM SWE product.  
16 The results show that it is feasible to utilize a ridge regression model based on a machine learning algorithm to prepare SWE  
17 products on a global scale. We evaluated the accuracy of the RRM SWE product using hemispheric-scale snow course  
18 (HSSC) observational data and Russian snow survey data. The MAE, RMSE, R, and R<sup>2</sup> between the RRM SWE products  
19 and observed SWEs are 0.21, 25.37 mm, 0.89, and 0.79, respectively. The accuracy of the RRM SWE dataset is improved by  
20 28%, 22%, 37%, 11%, and 11% compared with the original AMSR-E/AMSR2 (SWE), ERA-Interim SWE, Global Land  
21 Data Assimilation System (GLDAS) SWE, GlobSnow SWE, and ERA5-land SWE datasets, respectively, and it has a higher  
22 spatial resolution. The RRM SWE product production method does not rely heavily on an independent SWE product; it takes  
23 full advantage of each SWE dataset, and it takes into consideration the altitude factor. **The MAE ranges from 0.16 for areas  
24 within <100 m elevation to 0.29 within the 800-900 m elevation range. The MAE is best in the Russian region and worst in**

25 the Canadian region. The RMSE ranges from 4.71 mm for areas within <100 m elevation to 31.14 mm within the >1000 m  
26 elevation range. The RMSE is best in the Finland region and worst in the Canadian region. This method has good stability, is  
27 extremely suitable for the production of snow datasets with large spatial scales, and can be easily extended to the preparation  
28 of other snow datasets. The RRM SWE product is expected to provide more accurate SWE data for the hydrological model  
29 and climate model and provide data support for cryosphere change and climate change studies. The RRM SWE product is  
30 available from ‘A Big Earth Data Platform for Three Poles’ (<http://dx.doi.org/10.11888/Snow.tpd.c.271556>) (Li et al., 2021).

## 31 **1 Introduction**

32 The IPCC (Intergovernmental Panel on Climate Change) AR6 (Sixth Assessment Report) notes that the Northern  
33 Hemisphere spring snow cover has greatly decreased since 1950, and the feedback effect of the climate system caused by  
34 this reduction is extremely large (Masson-Delmotte et al., 2021). In most land areas of the Northern Hemisphere, annual  
35 runoff is dominated by snowmelt, and accurately estimating the impacts of such a large amount of snowmelt runoff on  
36 ecosystems and human activities is of great significance (Barnett et al., 2005; Bintanja and Andry, 2017; Henderson et al.,  
37 2018). Whether through hydrometeorological simulation or global change research, the estimation of the energy budget and  
38 mass of snow is very difficult, so a set of highly accurate, long time series snow cover datasets is urgently needed to drive  
39 hydrometeorological simulations and land surface process models. Among them, snow water equivalent (SWE) data play an  
40 irreplaceable role as an important parameter of the land surface hydrological model and climate model.

41 At present, there are many forms of SWE data in the world. According to type, these data can be divided into site  
42 observational SWE, remote sensing SWE, reanalysis SWE, data assimilation SWE and model simulation SWE. The remote  
43 sensing SWEs are mainly AMSR-E (Kelly, 2009) and AMSR2 (Imaoka et al., 2010; Tedesco and Jeyaratnam, 2019). The  
44 reanalysis SWE was mainly based on the ERA-Interim (Dee et al., 2011), MERRA2 (Gelaro et al., 2017), MERRA land  
45 (Reichle et al., 2011), and ERA5-land (Muñoz Sabater, 2019; Balsamo et al., 2015) datasets. The data assimilation SWE  
46 mainly includes GlobSnow (Luoju et al., 2021) and the Global Land Data Assimilation System (GLDAS) (Rodell et al.,  
47 2004). The site observational SWE mainly includes the GHCN dataset (Menne et al., 2016) and HSSC data (Pulliainen et al.,

48 2020). However, the time ranges of AMSR-E and AMSR-E2 SWE are only from 2003 to the present, which is lacking in  
49 terms of time series. Similarly, the GlobSnow SWE dataset is also seriously lacking in time series. Although the reanalysis  
50 SWE data have good spatial and temporal continuity and high data integrity, their accuracy is poor, and the MAE is 0.65  
51 (Snauffer et al., 2016). The SWE data from stations and meteorological observations cannot meet the needs of  
52 hydrometeorological and climate change research. This is mainly because SWE from stations is discontinuous in time series  
53 and severely missing. Furthermore, hydrometeorological studies often require spatiotemporally continuous grid data to be  
54 derived (Pan et al., 2003). There are great differences among remote-sensing SWE, reanalysis SWE data, data assimilation  
55 SWE and observational SWE. For remote-sensing SWE, the spatiotemporal characteristics of different passive microwave  
56 SWE data differ significantly due to differences in sensors or retrieval algorithms (Mudryk et al., 2015a). Data assimilation  
57 SWE and reanalysis SWE data also tend to exhibit different spatiotemporal characteristics due to differences in model  
58 design, driving data, and assimilation methods (Vuyovich et al., 2014). In summary, although there are a variety of SWE data  
59 in the world, the data quality is uncertain.

60 Previous studies have shown that all kinds of SWE data in the Northern Hemisphere have advantages and disadvantages,  
61 and none of these data perform well in all aspects (Mortimer et al., 2020). An effective method was applied in a study by  
62 Pulliainen et al. (Pulliainen et al., 2020), who applied a bias correction to GlobSnow and reanalysis data products based on  
63 SWE snow course measurements to obtain improved estimates on annual peak snow mass and SWE in the Northern  
64 Hemisphere. Another effective method is to fuse all kinds of SWE data in time and space, integrate the advantages of all  
65 kinds of data, and then generate a relatively complete SWE dataset. Many scholars have conducted in-depth studies on SWE  
66 data fusion. The main fusion methods can be classified into the following categories: multiproduct direct averaging (Mudryk  
67 et al., 2015b), linear regression (Snauffer et al., 2016), data assimilation (Pulliainen, 2006), “multiple” collocation (Pan et al.,  
68 2015) and machine learning (Snauffer et al., 2018; Xiao et al., 2018; Wang et al., 2020). Studies have shown that even the  
69 simplest multisource data average is more accurate than a single SWE product (Snauffer et al., 2018). However, the simple  
70 multisource data average cannot highlight the advantages of high-precision data, and it is easily affected by the weight ratio  
71 of low-precision data, which reduces the accuracy of fused data (Mudryk et al., 2015a). Although the linear regression  
72 method can make good use of the actual observational data to correct the original data, it is easy to overfit and causes the

73 overall deviation (Snauffer et al., 2016). The “multiple” collocation method changes the size of the original SWE data before  
74 fusion, which easily causes data errors. The data assimilation method is sensitive to the accuracy of input data, and it is  
75 difficult to fuse multisource data (Pan et al., 2015). In recent years, machine learning methods have been widely used in data  
76 fusion (Santi et al., 2021; Ntokas et al., 2021). Machine learning methods can not only integrate the advantages of  
77 multisource data but also make full use of site observational data to train the sample data, which easily generates SWE data  
78 products with large spatial scales and long time series (Broxton et al., 2019; Bair et al., 2018).

79 In summary, based on the existing SWE data products, combining a machine learning algorithm to fuse multisource SWE  
80 data is an effective method to prepare SWE products with long time series and large spatial scales and retain the advantages  
81 of single SWE data products. The ridge regression model is a biased estimation method specifically designed to address the  
82 problem of multicollinear data (Duzan and Shariff, 2015; Saleh et al., 2019). It has good tolerance to "ill-conditioned" data  
83 and has a good effect in using SWE data to address the multicollinearity problem (Hoerl and Kennard, 1970b; Guilkey and  
84 Murphy, 1975). In this study, we integrated multisource SWE data products of the RRM SWE based on the ridge regression  
85 model of the machine learning algorithm. We selected ERA-Interim SWE, GLDAS SWE, GlobSnow SWE, AMSR-  
86 E/AMSR2 SWE, and ERA5-land SWE data with relatively complete time series as the original data for the production of the  
87 RRM SWE product. The missing parts of the ERA-Interim SWE, AMSR-E/AMSR2 SWE, and GlobSnow SWE data were  
88 filled by the spatiotemporal interpolation method. The HSSC dataset (Pulliainen et al., 2020) and Russian snow survey data  
89 (Bulygina et al., 2011) were used as training sample data of "true SWE", and the effect of altitude on the algorithm was also  
90 considered. Thus, we prepared a set of spatiotemporal seamless SWE datasets (RRM SWE) covering the land region above  
91 45° N from 1979 to 2019. The spatial coverage of the RRM SWE product covers all land regions north of 45° N.

## 92 **2 Data and methods**

### 93 **2.1 Research region**

94 The research region of the RRM SWE product is located in the land region north of 45° N (Fig. 1). This region consists of  
95 Asia, Europe, and North America. The land region covers Russia, the United States, Canada, Denmark, Norway, Iceland,

96 Sweden, and Finland. This region has a cold climate and a wide area of snow cover.

## 97 **2.2 Grid SWE data description**

98 In this study, we utilized ERA-Interim SWE data (Dee et al., 2011), GLDAS SWE data (Rodell et al., 2004), GlobSnow  
99 SWE data (Luojus et al., 2021), AMSR-E/AMSR2 SWE data (Tedesco and Jeyaratnam, 2019), and ERA5-land SWE data  
100 (Muñoz Sabater, 2019) as the original input datasets for the fusion data (Table 1).

101 GlobSnow is a dataset of global snow cover and SWEs for the Northern Hemisphere released by the European Space  
102 Agency (ESA) (<http://www.globsnow.info/swe/>) (Luojus et al., 2021; Pulliainen et al., 2020). The SWE products in this  
103 dataset combine the Canadian Meteorological Center (CMC) daily snow depth analysis data (Walker et al., 2011), ground  
104 weather site observational data, and satellite microwave radiometer data. We obtained the L3A\_daily\_SWE product of this  
105 dataset. The temporal resolution of the L3A\_daily\_SWE product is daily, the spatial resolution is 0.25°, and the data format  
106 is NETCDF4.

107 ERA-Interim is the fourth generation reanalysis data of the European Centre for Medium-Range Weather Forecasts  
108 (ECMWF) (Dee et al., 2011). The data provide a global assimilated numerical product of various surface and top  
109 atmospheric parameters from January 1979 to the present ([https://apps.ecmwf.int/datasets/data/interim-full-  
110 daily/levtype=sfc/](https://apps.ecmwf.int/datasets/data/interim-full-daily/levtype=sfc/)). We obtained the SWE dataset with a daily temporal resolution, a spatial resolution of 0.25°, and  
111 NETCDF4 data format. The spatial range of the data is the land region above 45° N.

112 The Advanced Microwave Scanning Radiometer-Earth Observation System (AMSR-E) is a microwave scanning  
113 radiometer on the Aqua satellite of the National Aeronautics and Space Administration (NASA) Earth Observation System  
114 (EOS) (Tedesco and Jeyaratnam, 2019). The AMSR-E provides a global daily SWE dataset from June 19, 2002, to October  
115 3, 2011 ([https://nsidc.org/data/ae\\_dysno](https://nsidc.org/data/ae_dysno)). AMSR2 is a microwave scanning radiometer on the GCOM-W1 satellite launched  
116 by the Japan Aerospace Exploration Agency (JAXA) in May 2012. AMSR2 provides a global SWE dataset from July 2,  
117 2012, to the present ([https://nsidc.org/data/AU\\_DySno/versions/1](https://nsidc.org/data/AU_DySno/versions/1)). The spatial resolution of the AMSR-E SWE and AMSR2  
118 SWE datasets is 25 km x 25 km, the temporal resolution is daily, and the data formats are HDF-EOS and HDF-EOS5,  
119 respectively.

120 The GLDAS is a model used to describe global land information; it contains data, such as global rainfall, water  
121 evaporation, surface runoff, underground runoff, soil moisture, surface snow cover distribution, temperature, and heat flow  
122 distribution (Rodell et al., 2004). This assimilation system includes data with spatial resolutions of  $1^{\circ}\times 1^{\circ}$  and  $0.25^{\circ}\times 0.25^{\circ}$   
123 and temporal resolutions of 3 hours, 1 day and 1 month. The GLDAS data are available for download from the Goddard  
124 Earth Sciences Data and Information Services Center (GES DISC). We obtain an SWE dataset with a daily temporal  
125 resolution,  $0.25^{\circ}$  spatial resolution, and NETCDF4 data format.

126 ERA5-land is a reanalysis dataset that provides the evolution of global land parameter data since 1981 (Muñoz Sabater,  
127 2019). The dataset provides eight types of snow parameter data, including snow albedo, snow cover, snow depth, snowfall,  
128 the temperature of the snow layer, snowmelt, snow density, and SWE. This dataset provides a global SWE dataset with an  
129 hourly spatial resolution, a temporal resolution of  $0.1^{\circ}\times 0.1^{\circ}$ , a temporal coverage of January 1981 to the present, and data  
130 formats of GRIB and NETCDF4.

131 To maintain consistency in the spatial and temporal resolutions of the fused data, we unified the ERA-Interim SWE data,  
132 GLDAS SWE data, GlobSnow SWE data, AMSR-E/AMSR2 SWE data, and ERA5-land SWE data into a daily temporal  
133 resolution, with a spatial resolution of  $0.25^{\circ}$  and geographic projection of the North Pole Lambert azimuthal equal area.

### 134 **2.3 Ridge regression machine learning algorithm for preparing the SWE**

135 In this study, we utilize the ridge regression model of a machine learning algorithm to fuse ERA-Interim SWE data (Dee et  
136 al., 2011), GLDAS SWE data (Rodell et al., 2004), GlobSnow SWE data (Luo et al., 2021), AMSR-E/AMSR2 SWE data  
137 (Tedesco and Jeyaratnam, 2019), and ERA5-land SWE data (Muñoz Sabater, 2019) to generate a set of new RRM SWE  
138 datasets. The target reference data in this study are the HSSC dataset and Russian snow survey data. The digital elevation  
139 model (DEM) was used as an important environmental feature input to the ridge regression model and was included in the  
140 model training. The DEM is an auxiliary terrain feature variable in addition to the five SWE prediction feature variables,  
141 AMSR-E/AMSR2 SWE, ERA-Interim SWE, GLDAS SWE, GlobSnow SWE, and ERA5-land SWE.

142 The ridge regression model is a biased estimate regression method for collinear data analysis (Friedman et al., 2010; Hoerl  
143 and Kennard, 1970b, a). By abandoning the unbiasedness of the ordinary least squares, this algorithm can obtain the

144 regression method in which the regression coefficient is more practical and reliable at the cost of losing part of the  
 145 information and reducing the accuracy. The ridge regression model is flexible in the choice of predictor variables and does  
 146 not require the predictor and target variables to be independent of each other. It can effectively solve the multicollinearity  
 147 problem of predictor and target variables as well as reduce the impact of this problem on the training model (Duzan and  
 148 Shariff, 2015; Saleh et al., 2019). Generally, reanalysis data based on SWE products cannot make the products and models  
 149 independent of each other, i.e., they are prone to multicollinearity, which leads to distorted model estimation or difficulty in  
 150 performing accurate estimations. In contrast, the ridge regression model can successfully solve the multicollinearity problem,  
 151 i.e., the independence of training products and models. In addition, when integrating multiple SWE products, the accuracy of  
 152 each SWE dataset is likely to differ. A small change in one of the SWE products involved in the training will cause a  
 153 significant error in the final calculation results, while the ridge regression model has high accuracy and stability for these  
 154 "ill-conditioned" SWE data. In addition, the main advantage of this model is that SWE products with long time series and  
 155 large spatial scales are easy to prepare. The principle equation of the ridge regression model is defined as follows:

$$156 \quad \hat{\beta}^{ridge} = \underset{\beta}{\operatorname{argmin}} \left\{ \sum_{i=1}^N \left( y_i - \beta_0 - \sum_{j=1}^p x_{ij} \beta_j \right)^2 + \lambda \sum_{j=1}^p \beta_j^2 \right\}, \quad (1)$$

157 where  $\hat{\beta}^{ridge}$  is the extremum solution function of ridge regression and  $p$  is the number of gridded SWE product variables  
 158 involved in training.  $x_i$  are the prediction feature variables, which contain two parts: one set contains the main feature  
 159 variables of the gridded SWE products, and the other part consists of the DEM auxiliary feature variables.  $y_i$  is the observed  
 160 SWE, and  $\lambda$ ,  $\beta$ ,  $\beta_j$  and  $\beta_0$  are the parameters to be solved.  $1, \dots, N$  is the sample of the training dataset.  $\lambda \sum_{j=1}^p \beta_j^2$  is the  
 161 penalty function term. The total number of samples  $N$  in the training dataset is 271651. The sample sizes of the training  
 162 dataset, validation dataset and test dataset are divided according to the ratio of 7:2:1, where the numbers of training set,  
 163 validation set and test set samples are 271651, 77614 and 38807, respectively. The model is developed in Python3, and the  
 164 model framework is based on the "scikit-learn" machine learning library (<https://scikit-learn.org/stable/index.html>). The code  
 165 is available upon request.

166 The integration process of the RRM SWE product (Fig. 2) is described as follows:

- 167 1) The original ERA-Interim SWE data, GLDAS SWE data, GlobSnow SWE data, AMSR-E/AMSR2 SWE data, ERA5-  
168 land SWE data, DEM data, unified temporal resolution, spatial resolution, projection, spatial range, and unit are  
169 preprocessed.
- 170 2) The spatiotemporal interpolation method is used to fill in the missing data of AMSR-E/AMSR2 SWE, ERA-Interim  
171 SWE, and GlobSnow SWE in space and time. Based on this method, the missing AMSR-E/AMSR2 SWE data at low  
172 latitudes and the missing ERA-Interim SWE and GlobSnow SWE data in the time series are added.
- 173 3) The SWE data observed at stations from 1979 to 2014 are used as sample training data, and the AMSR-E/AMSR2  
174 SWE, ERA-Interim SWE, GLDAS SWE, GlobSnow SWE, ERA5-land SWE data, and DEM data are input into the  
175 ridge regression model of a machine learning algorithm for training. **During the RRM model training process, we  
176 reconstructed the training data to try to extract training samples that are uniformly distributed spatially as much as  
177 possible. First, a scan window of 250 km × 250 km (10 × 10 pixels) was created. Then, each gridded SWE data point  
178 participating in training is scanned, and the sample numbers in each scan window are counted. Finally, the mean value  
179  $n$  of the sample numbers in all scan windows is taken as the number of training samples to be selected in each scan  
180 window. For the scan window with sample numbers higher than  $n$ ,  $n$  samples are randomly selected from the scan  
181 window. For the scan window with sample numbers lower than  $n$ , all samples in the scan window are selected as  
182 training samples.**
- 183 4) When the model was trained, ERA-Interim SWE, GLDAS SWE, GlobSnow SWE, and ERA5-land SWE were used as  
184 the training data between 1979 and 2002 (AMSR-E/AMSR2 SWE data were not available before 2002), and AMSR-  
185 E/AMSR2 SWE, ERA-Interim SWE, GLDAS SWE, GlobSnow SWE, and ERA5-land SWE were used as the training  
186 data after 2002.
- 187 5) Based on the S-fold cross-validation method, the SWE data are continuously trained and validated, and the optimal  
188 model and parameters are finally selected and evaluated by the loss function.
- 189 6) Based on the trained optimal model, multiple SWE data products are integrated into the time series, missing data are  
190 predicted, and a set of spatiotemporally seamless SWE datasets is generated.



191 7) SWE data observed at stations from 2015 to 2018 are used to evaluate the accuracy of the RRM SWE product.

## 192 **2.4 Site data and evaluation metrics**

### 193 **2.4.1 Site SWE data for training, validation, and testing**

194 Russian snow survey data (<http://aisori.meteo.ru/ClimateR>) include the average snow depth data and the average snow  
195 density data of the station, and the SWE is the product of the measured average snow depth and average snow density  
196 (Bulygina et al., 2011). We obtained SWE data from 19493 stations from 1979-2016 from this dataset.

197 Hemispheric-scale snow course (hereafter referred to as HSSC) observational data are contained in a hemispheric-scale  
198 SWE database based on SWE observational datasets from the former Soviet Union/Russia (FSU), Finland, and Canada  
199 developed by Pulliainen et al. (Pulliainen et al., 2020; Bronnimann et al., 2018; Brown et al., 2019). This dataset is from the  
200 website of the Finnish Meteorological Institute (FMI) ([https://www.globsnow.info/swe/archive\\_v3.0/auxiliary\\_data/](https://www.globsnow.info/swe/archive_v3.0/auxiliary_data/)). The  
201 dataset provides data from 2687 distributed regional snow course observations and contains 343,241 SWE observational data  
202 points from 1979 to 2018. **The snow courses of the HSSC dataset are transects in which SWE is sampled manually at  
203 multiple locations with typical conditions to eliminate uncertainty in the regional-scale spatial variability of SWE due to the  
204 influence of snowpack characteristics and land cover type (Pulliainen et al., 2020).**

205 We carefully screened the Russian snow survey data and HSSC data and eliminated some abnormal observational data to  
206 ensure the high quality of the training, validation, and test sets. The null and zero values are removed during the HSSC data  
207 screening process. The null values, negative numbers, and extreme SWE values greater than 2000 mm are removed during  
208 the Russian snow survey data screening process.

### 209 **2.4.2 Accuracy evaluation method for datasets**

210 Mean absolute error (MAE), root mean square error (RMSE), Pearson's correlation coefficient (R), and coefficient of  
211 determination ( $R^2$ ) are used to evaluate the accuracies of AMSR-E/AMSR2 SWE, ERA-Interim SWE, GLDAS SWE,  
212 GlobSnow SWE, ERA5-land SWE, multisource data-averaged SWE, and the RRM SWE product. The specific equation of  
213 accuracy evaluation error is described as follows.

$$214 \quad MAE = \frac{1}{n} \sum_{i=1}^n |f_i - y_i|, \quad (2)$$

$$215 \quad RMSE = \left[ \frac{\sum_{i=1}^n (f_i - y_i)^2}{n} \right]^{\frac{1}{2}}, \quad (3)$$

$$216 \quad R = \frac{1}{n-1} \sum_{i=1}^n \left( \frac{f_i - \bar{f}}{\sigma_f} \right) \left( \frac{y_i - \bar{y}}{\sigma_y} \right), \quad (4)$$

$$217 \quad R^2 = \frac{\sum_{i=1}^n (f_i - \bar{f})^2}{\sum_{i=1}^n (y_i - \bar{y})^2}, \quad (5)$$

218 where  $n$  is the number of samples in the validation dataset,  $f_i$  is the SWE dataset product, and  $y_i$  is the measured SWE at  
 219 the station.  $\bar{f}$  and  $\bar{y}$  are the averages of SWE products and measured SWEs, respectively.  $\sigma_f$  and  $\sigma_y$  are the standard  
 220 deviation of SWE products and measured SWEs, respectively.

221 To further evaluate the accuracy of the RRM SWE dataset at the spatial scale, we compared it with AMSR-E/AMSR2  
 222 SWE, ERA-Interim SWE, GLDAS SWE, GlobSnow SWE, and ERA5-Land SWE at different altitude gradients. We also  
 223 evaluated MAE, RMSE, R and  $R^2$  separately for 11 elevation intervals: <100 m, 100-200 m, 200-300 m, 300-400 m, 400-  
 224 500 m, 500-600 m, 600-700 m, 700-800 m, 800-900 m, 900-1000 m, and >1000 m. In addition, we evaluated the  
 225 performances of the RRM SWE product in three representative regions: Russia, Canada, and Finland.

226 We used the Mann-Kendall trend test (Mann, 1945; Kendall, 1990) method to evaluate the variation trend in the RRM  
 227 SWE dataset from 1979 to 2019 and analyzed its reliability in terms of time series. Since the AMSR-E/AMSR2 SWE  
 228 product and the GlobSnow SWE product lack SWE data for Greenland, we removed the Greenland data to maintain  
 229 consistency in the spatial extent of the comparison data.

## 230 **3 Results and discussion**

### 231 **3.1 Overall accuracy evaluation of the RRM SWE product**

232 In this study, the accuracies of the RRM SWE, AMSR-E/AMSR2 SWE, ERA-Interim SWE, GLDAS SWE, GlobSnow  
233 SWE, and ERA5-land SWE were compared using test datasets from 2015 to 2018. MAE, RMSE, R, and  $R^2$  were used to  
234 reflect the data quality of each SWE product. In addition, we compared the RRM SWE product with the SWE dataset  
235 obtained by the multisource data average method.

236 According to the verification results in Fig. 3 and Table 2, the RRM SWE data have the best overall accuracy, and the  
237 MAE, RMSE, R, and  $R^2$  between the observed SWEs are 0.21, 25.37 mm, 0.89, and 0.79, respectively. The overall accuracy  
238 of the GlobSnow SWE and ERA5-land SWE products is higher than that of other SWE products. The overall deviation of  
239 the ERA5-land SWE products is the smallest except for the RRM SWE data, with MAE and RMSE values of 0.32 and 37.02  
240 mm, respectively. The correlation between the ERA5-land SWE and observed SWE is the highest except for the RRM SWE  
241 data, with R and  $R^2$  values of 0.84 and 0.71, respectively. Although the overall deviation between the GlobSnow SWE  
242 dataset and the measured SWE is small, its correlation with the measured value is low. The overall deviation between the  
243 ERA5-land SWE dataset and the measured SWE is higher than that of the GlobSnow SWE dataset, but its estimation  
244 accuracy for the high-value region of the SWE is low. In addition, the overall accuracy of the ERA-Interim SWE dataset and  
245 GLDAS SWE dataset is relatively low, but their integrities are higher than those of the GlobSnow SWE dataset and AMSR-  
246 E/AMSR2 SWE dataset in terms of temporal and spatial series. The AMSR-E/AMSR2 SWE dataset has a higher estimation  
247 accuracy for the low-value SWE region. Moreover, in the land region above  $45^\circ$  N, most of the existing SWE data products  
248 with regard to temporal and spatial degrees are missing to various degrees. Obviously, the accuracies of the existing SWE  
249 products were uneven, as no type of SWE dataset is perfect.

250 The verification results also indicate the following ranking orders:

251 The MAE ranking order is RRM SWE < GlobSnow SWE = ERA5-land SWE < ERA-Interim SWE < multisource data  
252 average SWE < AMSR-E/AMSR2 SWE < GLDAS SWE.

253 The RMSE ranking order is RRM SWE < ERA5-land SWE < GlobSnow SWE < ERA-Interim SWE < multisource data

254 average SWE < AMSR-E/AMSR2 SWE < GLDAS SWE.

255 The R ranking order is RRM SWE > ERA5-land SWE > GlobSnow SWE > ERA-Interim SWE > GLDAS SWE >  
256 multisource data average SWE > AMSR-E/AMSR2 SWE.

257 The R<sup>2</sup> ranking order is RRM SWE > ERA5-land SWE > GlobSnow SWE > ERA-Interim SWE > GLDAS SWE >  
258 multisource data average SWE > AMSR-E/AMSR2 SWE.

259 Compared with the ERA-Interim SWE, AMSR-E/AMSR2 SWE, GLDAS SWE, GlobSnow SWE, ERA5-land SWE, and  
260 multisource data average SWE, the MAE of the RRM SWE and observed SWE is reduced by 0.22, 0.28, 0.37, 0.11, 0.11 and  
261 0.23, respectively. The RMSE of the RRM SWE and observed SWE is reduced by 21.44 mm, 27.02 mm, 39.88 mm, 15.62  
262 mm, 11.65 mm, and 26.63 mm, respectively. The correlation coefficients of the RRM SWE and observed SWE are improved  
263 by 0.20, 0.42, 0.37, 0.19, 0.05, and 0.38, respectively. The coefficient of determination of the RRM SWE and observed SWE  
264 is improved by 0.31, 0.57, 0.52, 0.30, 0.08, and 0.53, respectively. Although the multisource data average method can  
265 improve the accuracy of SWE products to some extent (better than AMSR-E/AMSR2 SWE and GLDAS SWE), the  
266 improvement of this method is still very limited. **The RRM SWE product has a significant advantage over the multisource  
267 data average method, and its accuracy is much higher than that of the simple multisource data average method (Table 2).  
268 Based on the above verification results, the accuracy of the RRM SWE is significantly improved; the RRM SWE dataset has  
269 higher accuracy than that of any single grid SWE dataset, and it also fills the gap in the original SWE data in terms of spatial  
270 and temporal resolutions.**

271 Based on the kernel density estimation method, we analyzed the density distribution of different SWE datasets (Fig. 4).  
272 The results show that the RRM SWE dataset is closer to the 1:1 line and has the highest accuracy. The RRM SWE dataset is  
273 particularly accurate for SWE estimation in the low-value region, and the test data are concentrated near the 1:1 line in the  
274 high-density region (kernel density estimation > 0.00015) (Fig. 4). In contrast, the high-density regions of the GLDAS SWE  
275 dataset, ERA-Interim SWE dataset, and AMSR-E/AMSR2 SWE dataset deviate significantly from the 1:1 line, resulting in  
276 poor accuracy. The AMSR-E/AMSR2 SWE, GLDAS SWE, and GlobSnow SWE are underestimated relative to the SWE  
277 measured at the site, among which GLDAS SWE underestimated the observed SWE the most seriously, while ERA5-land  
278 SWE overestimated the observed SWE. Although the accuracies of GlobSnow SWE and ERA5-land SWE are relatively

279 high, their dispersion degrees are large (the kernel density estimation for most test data is less than 0.0001). Overall, the  
280 RRM SWE data have a higher overall estimation accuracy, especially for the low-value area of SWE. For an SWE above  
281 400 mm, the MAE and RMSE of the RRM SWE product and the measured SWE are 0.35 and 43.57 mm, respectively.  
282 The estimation accuracy of the RRM SWE product for the high value range of SWE (SWE > 400 mm) is lower than that for  
283 the low value range of SWE (SWE < 400 mm) (Fig. 4). The main reason for this is that the training accuracy of the RRM  
284 model for the high-value range of SWE is affected by the small number of stations that observe the high-value range of  
285 SWE.

286 However, in this study, there are still some uncertainties in the ridge regression machine learning algorithm that integrates  
287 SWE products. First, this model is strongly dependent on on-site observational data, and the fusion precision of SWE is poor  
288 in some areas with sparse observational stations. The fusion accuracy of SWE products will be affected to a certain extent  
289 without considering the prior snow cover information. The RRM SWE product is still underestimated in cases of high SWE.  
290 Then, in addition to the DEM, meteorological elements, NDVI, land type, and other factors will affect the SWE estimation.  
291 Unfortunately, our current RRM presented here does not consider these factors as predictors, which is a limitation of the  
292 current RRM SWE product. Finally, in complex terrain with an elevation interval >1000 m, the RRM SWE product  
293 performed poorly, with an RMSE of 31.14 mm (Fig. 5), and the integration of SWE products remains challenging (Mortimer  
294 et al., 2020).

### 295 3.2 Accuracy evaluation of the RRM SWE product at different altitudes and regions

296 The accuracy of each SWE product is not absolute at different altitude gradients based on evaluations of the AMSR-  
297 E/AMSR2 SWE, ERA-Interim SWE, GLDAS SWE, GlobSnow SWE, and ERA5-land SWE product accuracies (Fig. 5).  
298 The accuracy of a single SWE product is different from its overall accuracy. We consider the influence of altitude in the  
299 algorithm and make full use of the accuracy advantage of each SWE data for different altitude gradients.

300 The above verification results show that the MAE, RMSE, R and R<sup>2</sup> between the RRM SWE product and measured SWE  
301 perform well at altitude gradients of <100 m, 100-200 m, 200-300 m, 300-400 m, 400-500 m, 500-600 m, 600-700 m, 700-  
302 800 m, 800-900 m, 900-1000 m and >1000 m (Fig. 5). Overall, the RRM SWE product has the highest accuracy in the

303 elevation intervals of <100 m, 100-200 m, 200-300 m, 400-500 m, 500-600 m, 600-700 m, 700-800 m, 800-900 m,  
304 and >1000 m. The RRM SWE product itself has the best performance in the elevation interval <100 m. The ERA5-land  
305 product has the best performance in the elevation interval 300-400 m. The GlobSnow product has the best performance in  
306 the elevation interval 900-1000 m.

307 The RRM SWE product has good performance in different regions, and its RMSE in Russia, Canada, and Finland are  
308 26.39 mm, 29.31 mm, and 25.29 mm, respectively; additionally, the performance of the RRM SWE product in different  
309 regions is basically similar (Table 3). The RRM SWE product performs well not only at different altitudes but also in  
310 different regions, and it has good stability.

### 311 **3.3 Comparison of spatial distribution patterns between the RRM SWE product and traditional SWE products**

312 A comparison of the spatially distributed annual average SWE distributions is made between the RRM SWE and AMSR-  
313 E/AMSR2 SWE, ERA-Interim SWE, GLDAS SWE, GlobSnow SWE, and ERA5-land SWE in 2014, 2015, 2016, and 2017,  
314 and their spatial distribution patterns are shown in Fig. 6.

315 Overall, the RRM SWE dataset, AMSR-E/AMSR2 SWE dataset, ERA-Interim SWE dataset, GLDAS SWE dataset,  
316 GlobSnow SWE dataset, and ERA5-land SWE dataset have similar spatial distribution patterns in the land region above 45°  
317 N, showing a trend of lower SWE in low latitudes and higher SWE in high latitudes. The AMSR-E/AMSR2 SWE dataset  
318 covers a limited extent in the land region above 45° N, many data points are missing, and low SWE values exist at low  
319 latitudes. In northern Siberia, the ERA-Interim SWE product has a higher SWE, and there are many abnormal, extreme SWE  
320 values (SWE > 500 mm) in this dataset. In low-latitude regions, such as Alaska, North Siberia, and the easternmost region of  
321 Russia, the SWE of GLDAS SWE products is significantly lower. The GlobSnow SWE product lacks SWE data for  
322 Greenland, and this dataset has low SWEs in the Baffin Island, Koryak Mountains, Kamchatka Peninsula, and Alaska  
323 regions. The ERA5-land SWE products have low SWEs in northeastern Russia, Scandinavia, and northeastern Canada. The  
324 RRM SWE dataset is more reasonable for estimating the spatial distribution of SWE in the land region above 45° N, and the  
325 data integrity is higher. Moreover, based on the new machine learning algorithm, a variety of SWE data products in different  
326 time series are fused, which makes the RRM SWE dataset completely temporally and spatially continuous.

327 The relative difference between the RRM SWE data and GLDAS SWE data is the highest, and the relative difference is  
328 greater than 80% in most low altitude regions (Fig. 7). The relative difference between the RRM SWE data and the  
329 GlobSnow SWE data is relatively small overall, especially in most high-latitude areas where the relative difference is less  
330 than 10% (Fig. 7). Overall, the annual average relative differences in the RRM SWE data and AMSR2 SWE, ERA-Interim  
331 SWE, GLDAS SWE, GlobSnow SWE, and ERA5-land SWE are 37%, 41%, 54%, 25%, and 29%, respectively (Fig. 7).  
332 Previous studies have shown that the accuracy of the SWE in the Northern Hemisphere estimated by GlobSnow SWE data is  
333 higher (Pulliainen et al., 2020), while the spatial distribution pattern of the RRM SWE data is close to the estimation result of  
334 GlobSnow SWE. In addition, the single point verification results based on the measured SWE data of meteorological stations  
335 in section 3.1 show that the RRM SWE dataset has higher accuracy than the GlobSnow SWE dataset. The RRM SWE  
336 dataset has good accuracy.

### 337 **3.4 Comparison of the annual variation tendencies of AMSR-E/AMSR2 SWE, ERA-Interim SWE, GLDAS SWE,** 338 **GlobSnow SWE, and ERA5-land SWE and the RRM SWE in the land region above 45° N**

339 Based on the Mann-Kendall trend test, we analyzed the changing trend in the region-wide annual average SWE of the  
340 AMSR-E/AMSR2 SWE, ERA-Interim SWE, GLDAS SWE, GlobSnow SWE, ERA5-land SWE, and RRM SWE in the land  
341 region above 45° N from 1979 to 2019.

342 Based on the Mann-Kendall trend test (see Fig. 8 and Table 4), from 1979 to 2019, the test value of the ERA-Interim  
343 region-wide annual average SWE is 1.08, and there is no significant change trend under the significance test level of 0.05.  
344 The test value of the GLDAS region-wide annual average SWE was 4.95 and showed a significant increasing trend at the  
345 significance test level of 0.05. The test values of the AMSR-E/AMSR2 annual average SWE, GlobSnow annual average  
346 SWE, ERA5-land annual average SWE, and RRM annual average SWE are -3.26, -2.54, -3.43, and -3.00, respectively, and  
347 these four SWEs showed a significant decreasing trend at the significance test level of 0.05. Based on the analysis of the  
348 RRM SWE product, between 1979 and 2019, the region-wide annual average SWE in the land region above 45° N decreased  
349 by 15.1 percent. In the Northern Hemisphere, spring snow cover extent has decreased significantly, according to the Fifth  
350 Assessment Report (AR5) of the IPCC. Between 1967 and 2010, the spring snow cover extent decreased by an average of

351 1.6 percent per decade, while the June snow cover extent decreased by 11.7 percent per decade (Stocker, 2014). Most studies  
352 have shown that the annual variation tendency of snow depth and snow cover extent showed a significant decreasing trend in  
353 the Northern Hemisphere (Brutel-Vuilmet et al., 2013), which is consistent with the annual variation tendency of the RRM  
354 SWE dataset. This dataset can reflect the characteristics of snow cover change in the land region above 45° N in light of  
355 climate change and can be used as the driving data for climate models to support climate change-related research. In  
356 addition, this dataset is expected to provide a snow data basis for the study of "Arctic amplification".

#### 357 **4 Data availability**

358 The RRM SWE product is available for free download from 'A Big Earth Data Platform for Three Poles'  
359 (<http://dx.doi.org/10.11888/Snow.tpd.271556>) (Li et al., 2021). The temporal resolution of the RRM SWE product is daily,  
360 and the spatial resolution is 10 km. It spans latitudes of 45°N-90°N and longitudes of 180°W-180°E. A brief summary and  
361 data description document (including data details, spatial range, and usage method) are also provided.

#### 362 **5 Conclusions**

363 In this study, we propose a method to fuse multisource SWE data by a ridge regression model based on machine learning. A  
364 new method was utilized to prepare a set of spatiotemporally seamless SWE datasets of the RRM SWE, combined with the  
365 original AMSR-E/AMSR2 SWE, ERA-Interim SWE, GLDAS SWE, GlobSnow SWE, and ERA5-land SWE datasets. In the  
366 RRM SWE dataset, the time series of the data is 1979-2019, the temporal resolution is daily, the spatial resolution is 10 km,  
367 and the spatial range is the land region above 45° N.

368 The RRM SWE data product has the best accuracy, especially for the estimation of low SWE. The accuracy ranking of the  
369 SWE dataset verified by the test dataset is described as follows: RRM SWE > ERA5-land SWE > GlobSnow SWE > ERA-  
370 Interim SWE > multisource data average SWE > AMSR-E/AMSR2 SWE > GLDAS SWE. The accuracy of the RRM SWE  
371 dataset is higher than that of the existing SWE products at most elevation intervals. The RRM SWE product has good  
372 performance and stability in different regions. Moreover, the RRM SWE dataset spatiotemporally fills in the missing data of



373 the original SWE dataset.

374 Compared with traditional fusion methods, machine learning methods have a strong advantage. We find that the simple  
375 machine learning algorithm has not only high efficiency but also good accuracy in the preparation of SWE products on a  
376 global scale. Without losing the advantages of existing SWE products, this method can also make full use of station  
377 observational data to integrate the advantages of various SWE products. The model training process does not rely too much  
378 on a specific sample, and this model has a strong generalization ability. In addition, the influence of altitude on the  
379 preparation scheme is considered in detail in the model. Compared with the SWE dataset prepared by the traditional method,  
380 the spatial resolution is only 25 km, while this new method obtains an SWE dataset with a higher spatial resolution of 10 km.

381 We propose that the RRM SWE dataset preparation scheme has good continuity and can prepare real-time and high-  
382 quality SWE datasets in the land region above 45° N. In addition, the new method proposed in this paper has the advantages  
383 of simplicity and high precision in preparing large-scale SWE datasets and can be easily extended to the preparation of other  
384 snow datasets. This dataset is an important supplement to the land region above the 45° N SWE database and is expected to  
385 provide data support for Arctic cryosphere studies and global climate change studies.

#### 386 **Author contributions.**

387 DS and HL designed the study and wrote the manuscript; JW, XH, and TC contributed to the discussions, edits, and  
388 revisions. DS and WJ compiled the model code.

#### 389 **Competing interests.**

390 The authors declare that they have no conflicts of interest.

#### 391 **Acknowledgments.**

392 The authors would like to thank the European Space Agency (ESA) for providing the GlobSnow data, the European Centre  
393 for Medium-Range Weather Forecasts (ECMWF) for ERA-Interim data and ERA5-land data, the National Aeronautics and

394 Space Administration (NASA) for the AMSR-E/AMSR2 data, the Goddard Earth Sciences Data and Information Services  
395 Center (GESDISC) for the GLDAS data, the Russian Federal Service for Hydrometeorology and Environmental Monitoring  
396 (ROSHYDROMET) for the snow survey data, and the Finnish Meteorological Institute (FMI) for the hemispheric-scale  
397 snow course (HSSC) observational data.

#### 398 **Financial support.**

399 This research was supported by the Strategic Priority Research Program of the Chinese Academy of Sciences (Grant No.  
400 XDA19070302), the National Science Fund for Distinguished Young Scholars (Grant No. 42125604), and the National  
401 Natural Science Foundation of China (Grant No. 41971399, 41971325, 42171391).

#### 402 **References**

- 403 Bair, E. H., Abreu Calfa, A., Rittger, K., and Dozier, J.: Using machine learning for real-time estimates of snow water  
404 equivalent in the watersheds of Afghanistan, *The Cryosphere*, 12, 1579-1594, 2018.
- 405 Balsamo, G., Albergel, C., Beljaars, A., Boussetta, S., Brun, E., Cloke, H., Dee, D., Dutra, E., Munoz-Sabater, J.,  
406 Pappenberger, F., de Rosnay, P., Stockdale, T., and Vitart, F.: ERA-Interim/Land: a global land surface reanalysis data set,  
407 *Hydrol Earth Syst Sc*, 19, 389-407, 10.5194/hess-19-389-2015, 2015.
- 408 Barnett, T. P., Adam, J. C., and Lettenmaier, D. P.: Potential impacts of a warming climate on water availability in snow-  
409 dominated regions, *Nature*, 438, 303-309, 10.1038/nature04141, 2005.
- 410 Bintanja, R. and Andry, O.: Towards a rain-dominated Arctic, *Nat Clim Change*, 7, 263+, 10.1038/Nclimate3240, 2017.
- 411 Bronnimann, S., Allan, R., Atkinson, C., Buizza, R., Bulygina, O., Dahlgren, P., Dee, D., Dunn, R., Gomes, P., John, V. O.,  
412 Jourdain, S., Haimberger, L., Hersbach, H., Kennedy, J., Poli, P., Pulliainen, J., Rayner, N., Saunders, R., Schulz, J., Sterin,  
413 A., Stickler, A., Titchner, H., Valente, M. A., Ventura, C., and Wilkinson, C.: Observations for Reanalyses, *Bulletin of the*  
414 *American Meteorological Society*, 99, 1851-1866, 10.1175/Bams-D-17-0229.1, 2018.
- 415 Brown, R. D., Fang, B., and Mudryk, L.: Update of Canadian historical snow survey data and analysis of snow water

416 equivalent trends, 1967–2016, *Atmosphere-Ocean*, 57, 149-156, 2019.

417 Broxton, P. D., Van Leeuwen, W. J., and Biederman, J. A.: Improving snow water equivalent maps with machine learning of  
418 snow survey and lidar measurements, *Water Resources Research*, 55, 3739-3757, 2019.

419 Brutel-Vuilmet, C., Menegoz, M., and Krinner, G.: An analysis of present and future seasonal Northern Hemisphere land  
420 snow cover simulated by CMIP5 coupled climate models, *Cryosphere*, 7, 67-80, 10.5194/tc-7-67-2013, 2013.

421 Bulygina, O. N., Groisman, P. Y., Razuvaev, V. N., and Korshunova, N. N.: Changes in snow cover characteristics over  
422 Northern Eurasia since 1966, *Environmental Research Letters*, 6, Artn 04520410.1088/1748-9326/6/4/045204, 2011.

423 Dee, D. P., Uppala, S. M., Simmons, A., Berrisford, P., Poli, P., Kobayashi, S., Andrae, U., Balmaseda, M., Balsamo, G., and  
424 Bauer, d. P.: The ERA - Interim reanalysis: Configuration and performance of the data assimilation system, *Quarterly  
425 Journal of the royal meteorological society*, 137, 553-597, 2011.

426 Duzan, H. and Shariff, N. S. B. M.: Ridge regression for solving the multicollinearity problem: review of methods and  
427 models, *Journal of Applied Science*, 2015.

428 Friedman, J., Hastie, T., and Tibshirani, R.: Regularization Paths for Generalized Linear Models via Coordinate Descent, *J  
429 Stat Softw*, 33, 1-22, DOI 10.18637/jss.v033.i01, 2010.

430 Gelaro, R., McCarty, W., Suarez, M. J., Todling, R., Molod, A., Takacs, L., Randles, C. A., Darmenov, A., Bosilovich, M. G.,  
431 Reichle, R., Wargan, K., Coy, L., Cullather, R., Draper, C., Akella, S., Buchard, V., Conaty, A., da Silva, A. M., Gu, W., Kim,  
432 G. K., Koster, R., Lucchesi, R., Merkova, D., Nielsen, J. E., Partyka, G., Pawson, S., Putman, W., Rienecker, M., Schubert,  
433 S. D., Sienkiewicz, M., and Zhao, B.: The Modern-Era Retrospective Analysis for Research and Applications, Version 2  
434 (MERRA-2), *J Climate*, 30, 5419-5454, 10.1175/Jcli-D-16-0758.1, 2017.

435 Guilkey, D. K. and Murphy, J. L.: Directed Ridge Regression Techniques in Cases of Multicollinearity, *J Am Stat Assoc*, 70,  
436 769-775, 1975.

437 Henderson, G. R., Peings, Y., Furtado, J. C., and Kushner, P. J.: Snow-atmosphere coupling in the Northern Hemisphere, *Nat  
438 Clim Change*, 8, 954-+, 10.1038/s41558-018-0295-6, 2018.

439 Hoerl, A. E. and Kennard, R. W.: Ridge regression: applications to nonorthogonal problems, *Technometrics*, 12, 69-82,  
440 1970a.

441 Hoerl, A. E. and Kennard, R. W.: Ridge regression: Biased estimation for nonorthogonal problems, *Technometrics*, 12, 55-  
442 67, 1970b.

443 Imaoka, K., Kachi, M., Fujii, H., Murakami, H., Hori, M., Ono, A., Igarashi, T., Nakagawa, K., Oki, T., Honda, Y., and  
444 Shimoda, H.: Global Change Observation Mission (GCOM) for Monitoring Carbon, Water Cycles, and Climate Change, *P*  
445 *Ieee*, 98, 717-734, 10.1109/Jproc.2009.2036869, 2010.

446 IPCC, 2021: Climate Change 2021: The Physical Science Basis. Contribution of Working Group I to the Sixth Assessment  
447 Report of the Intergovernmental Panel on Climate Change [Masson-Delmotte, V., P. Zhai, A. Pirani, S.L. Connors, C. Péan,  
448 S. Berger, N. Caud, Y. Chen, L. Goldfarb, M.I. Gomis, M. Huang, K. Leitzell, E. Lonnoy, J.B.R. Matthews, T.K. Maycock,  
449 T. Waterfield, O. Yelekçi, R. Yu, and B. Zhou (eds.)]. Cambridge University Press. In Press.

450 Kelly, R.: The AMSR-E Snow Depth Algorithm: Description and Initial Results, 2009.

451 Kendall, M. G.: Rank Correlation Methods, *British Journal of Psychology*, 25, 86–91, 1990.

452 Li, H., Shao, D., Li, H., Wang, W., Ma, Y., and Lei, H.: Arctic Snow Water Equivalent Grid Dataset (1979-2019), A Big  
453 Earth Data Platform for Three Poles [dataset], 10.11888/Snow.tpd.271556, 2021.

454 Luoju, K., Pulliainen, J., Takala, M., Lemmetyinen, J., Mortimer, C., Derksen, C., Mudryk, L., Moisander, M., Hiltunen,  
455 M., and Smolander, T.: GlobSnow v3. 0 Northern Hemisphere snow water equivalent dataset, *Scientific Data*, 8, 1-16, 2021.

456 Mann, H. B.: Nonparametric test against trend, *Econometrica*, 13, 245-259, 1945.

457 Menne, M., Durre, I., Korzeniewski, B., McNeal, S., Thomas, K., Yin, X., Anthony, S., Ray, R., Vose, R., and Gleason, B.:  
458 Global Historical Climatology Network–Daily (GHCN-Daily), Version, 3, V5D21VHZ, 2016.

459 Mortimer, C., Mudryk, L., Derksen, C., Luoju, K., Brown, R., Kelly, R., and Tedesco, M.: Evaluation of long-term Northern  
460 Hemisphere snow water equivalent products, *The Cryosphere*, 14, 1579-1594, 2020.

461 Mudryk, L., Derksen, C., Kushner, P., and Brown, R.: Characterization of Northern Hemisphere snow water equivalent  
462 datasets, 1981–2010, *Journal of Climate*, 28, 8037-8051, 2015a.

463 Mudryk, L. R., Derksen, C., Kushner, P. J., and Brown, R.: Characterization of Northern Hemisphere Snow Water Equivalent  
464 Datasets, 1981-2010, *J Climate*, 28, 8037-8051, 10.1175/Jcli-D-15-0229.1, 2015b.

465 Muñoz Sabater, J.: ERA5-Land hourly data from 1981 to present, Copernicus Climate Change Service (C3S) Climate Data

466 Store (CDS), 2019.

467 Ntokas, K. F., Odry, J., Boucher, M.-A., and Garnaud, C.: Investigating ANN architectures and training to estimate snow  
468 water equivalent from snow depth, *Hydrology and Earth System Sciences*, 25, 3017-3040, 2021.

469 Pan, M., Fisher, C. K., Chaney, N. W., Zhan, W., Crow, W. T., Aires, F., Entekhabi, D., and Wood, E. F.: Triple collocation:  
470 Beyond three estimates and separation of structural/non-structural errors, *Remote Sens Environ*, 171, 299-310,  
471 10.1016/j.rse.2015.10.028, 2015.

472 Pan, M., Sheffield, J., Wood, E. F., Mitchell, K. E., Houser, P. R., Schaake, J. C., Robock, A., Lohmann, D., Cosgrove, B.,  
473 and Duan, Q.: Snow process modeling in the North American Land Data Assimilation System (NLDAS): 2. Evaluation of  
474 model simulated snow water equivalent, *Journal of Geophysical Research: Atmospheres*, 108, 2003.

475 Pulliainen, J.: Mapping of snow water equivalent and snow depth in boreal and sub-arctic zones by assimilating space-borne  
476 microwave radiometer data and ground-based observations, *Remote Sens Environ*, 101, 257-269, 10.1016/j.rse.2006.01.002,  
477 2006.

478 Pulliainen, J., Luojus, K., Derksen, C., Mudryk, L., Lemmetyinen, J., Salminen, M., Ikonen, J., Takala, M., Cohen, J.,  
479 Smolander, T., and Norberg, J.: Patterns and trends of Northern Hemisphere snow mass from 1980 to 2018 (vol 41, pg 861,  
480 2020), *Nature*, 582, E18-E18, 10.1038/s41586-020-2416-4, 2020.

481 Reichle, R. H., Koster, R. D., De Lannoy, G. J. M., Forman, B. A., Liu, Q., Mahanama, S. P. P., and Toure, A.: Assessment  
482 and Enhancement of MERRA Land Surface Hydrology Estimates, *J Climate*, 24, 6322-6338, 10.1175/Jcli-D-10-05033.1,  
483 2011.

484 Rodell, M., Houser, P., Jambor, U., Gottschalck, J., Mitchell, K., Meng, C.-J., Arsenault, K., Cosgrove, B., Radakovich, J.,  
485 and Bosilovich, M.: The global land data assimilation system, *Bulletin of the American Meteorological Society*, 85, 381-394,  
486 2004.

487 Saleh, A. M. E., Arashi, M., and Kibria, B. G.: Theory of ridge regression estimation with applications, John Wiley &  
488 Sons 2019.

489 Santi, E., Brogioni, M., Leduc-Leballeur, M., Macelloni, G., Montomoli, F., Pampaloni, P., Lemmetyinen, J., Cohen, J., Rott,  
490 H., and Nagler, T.: Exploiting the ANN Potential in Estimating Snow Depth and Snow Water Equivalent From the Airborne

491 SnowSAR Data at X-and Ku-Bands, IEEE Transactions on Geoscience and Remote Sensing, 2021.

492 Snauffer, A. M., Hsieh, W. W., and Cannon, A. J.: Comparison of gridded snow water equivalent products with in situ  
493 measurements in British Columbia, Canada, J Hydrol, 541, 714-726, 10.1016/j.jhydrol.2016.07.027, 2016.

494 Snauffer, A. M., Hsieh, W. W., Cannon, A. J., and Schnorbus, M. A.: Improving gridded snow water equivalent products in  
495 British Columbia, Canada: multi-source data fusion by neural network models, Cryosphere, 12, 891-905, 10.5194/tc-12-891-  
496 2018, 2018.

497 Stocker, T.: Climate change 2013: the physical science basis: Working Group I contribution to the Fifth assessment report of  
498 the Intergovernmental Panel on Climate Change, Cambridge university press2014.

499 Tedesco, M. and Jeyaratnam, J.: AMSR-E/AMSR2 Unified L3 Global Daily 25 km EASE-Grid Snow Water Equivalent,  
500 Version 1.[online] Boulder, Colorado USA, NASA National Snow and Ice Data Center Distributed Active Archive Center,  
501 2019.

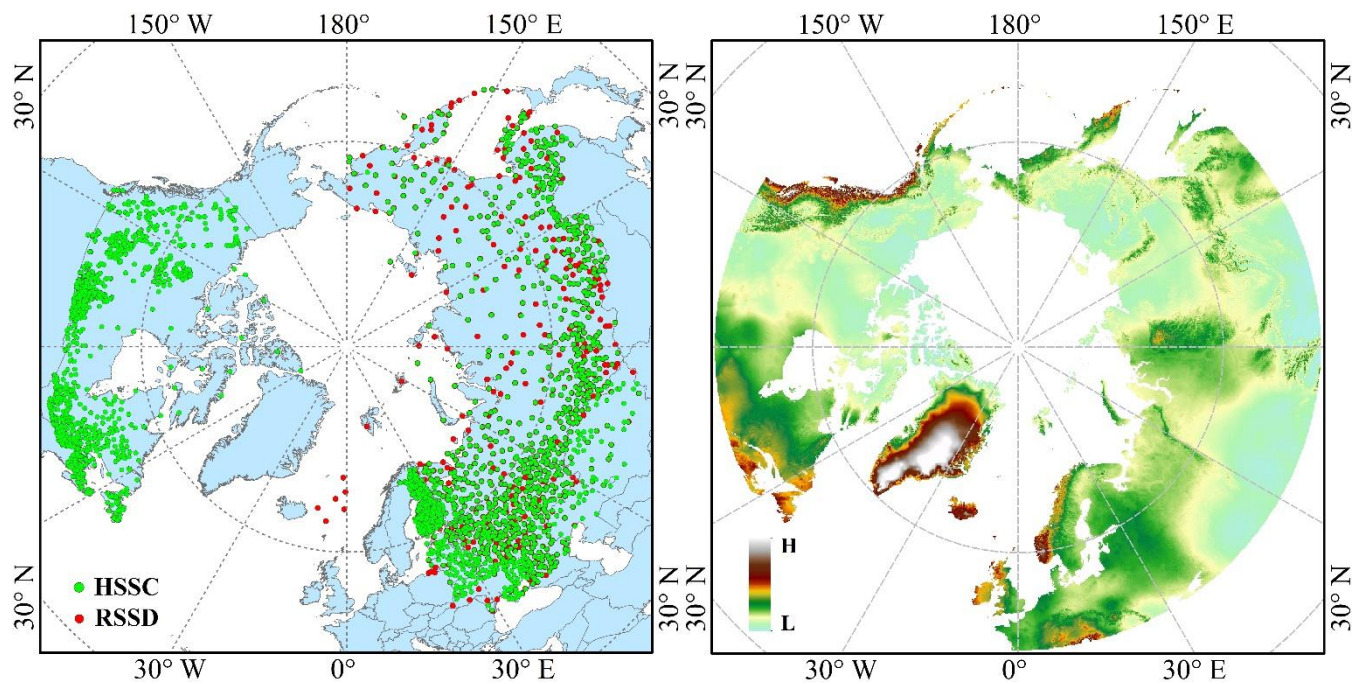
502 Vuyovich, C. M., Jacobs, J. M., and Daly, S. F.: Comparison of passive microwave and modeled estimates of total watershed  
503 SWE in the continental U nited S tates, Water resources research, 50, 9088-9102, 2014.

504 Walker, A., Brasnett, B., and Brown, R.: Canadian Meteorological Centre (CMC) daily gridded snow depth analysis for  
505 Northern Hemisphere, 1998-2008, 2011.

506 Wang, J. W., Yuan, Q. Q., Shen, H. F., Liu, T. T., Li, T. W., Yue, L. W., Shi, X. G., and Zhang, L. P.: Estimating snow depth  
507 by combining satellite data and ground-based observations over Alaska: A deep learning approach, J Hydrol, 585, ARTN  
508 12482810.1016/j.jhydrol.2020.124828, 2020.

509 Xiao, X. X., Zhang, T. J., Zhong, X. Y., Shao, W. W., and Li, X. D.: Support vector regression snow-depth retrieval algorithm  
510 using passive microwave remote sensing data, Remote Sens Environ, 210, 48-64, 10.1016/j.rse.2018.03.008, 2018.

511



512

513

**Figure 1: The DEM and snow survey stations of the research region. The right subgraph shows the DEM, and the left subgraph**

514

**shows the SWE observational stations. HSSC, hemispheric-scale snow course; RSSD, the Russian snow survey station. The spatial**

515

**range of the RRM SWE product is consistent with that of the DEM.**

516

517

**Table 1: Introduction to the SWE data.**

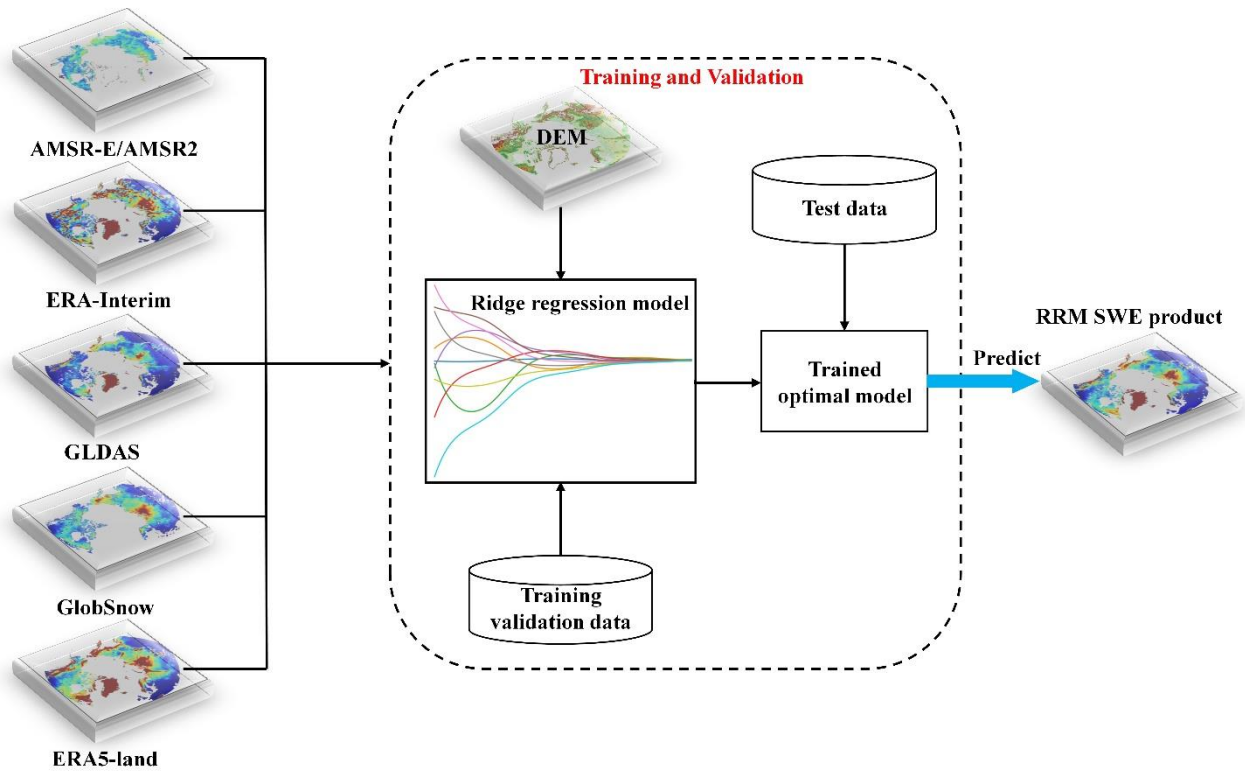
<b>Data type</b>	<b>Data name</b>	<b>Time series</b>	<b>Temporal resolution</b>	<b>Spatial resolution</b>	<b>Spatial coverage</b>	<b>File format</b>
Remote sensing data	AMSR-E/AMSR2	2002-2011/2012-2020	Daily	25 km x 25 km	Global (No Greenland)	HDF5
Data assimilation dataset	GLDAS	1979-2020	Daily	0.25°×0.25°	Global	NetCDF
	GlobSnow	1979-2018	Daily	0.25°×0.25°	Northern Hemisphere (No Greenland)	NetCDF
Reanalysis dataset	ERA-Interim	1979-2019	Daily	0.25°×0.25°	Global	NetCDF
	ERA5-land	1981- present	Hour	0.1°×0.1°	Global	NetCDF

519

520

521





522

523

Figure 2: Flow chart of the RRM SWE data preparation (preparation of spatiotemporal seamless SWE datasets mainly includes

524

three processes: model training, model reasoning, and SWE data preparation).

525

526

527 **Table 2: Error list for the station data and grid snow water equivalent products.**

<b>Error type</b>	<b>MAE</b>	<b>RMSE (mm)</b>	<b>R</b>	<b>R<sup>2</sup></b>
ERA-Interim	0.43	46.81	0.69	0.48
AMSR-E/AMSR2	0.49	52.39	0.47	0.22
GLDAS	0.58	65.25	0.52	0.27
GlobSnow	0.32	40.99	0.70	0.49
ERA5-land	0.32	37.02	0.84	0.71
Multisource data average	0.44	52.00	0.51	0.26
RRM SWE	0.21	25.37	0.89	0.79

528

529

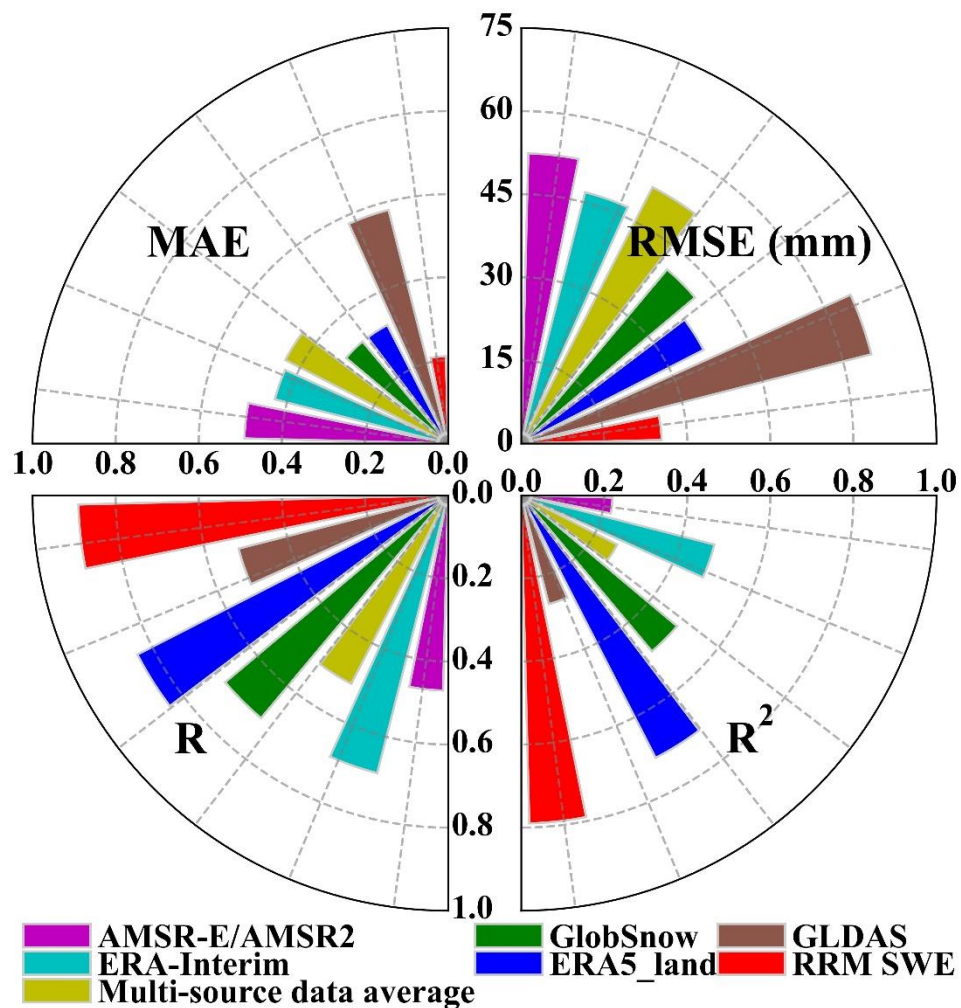
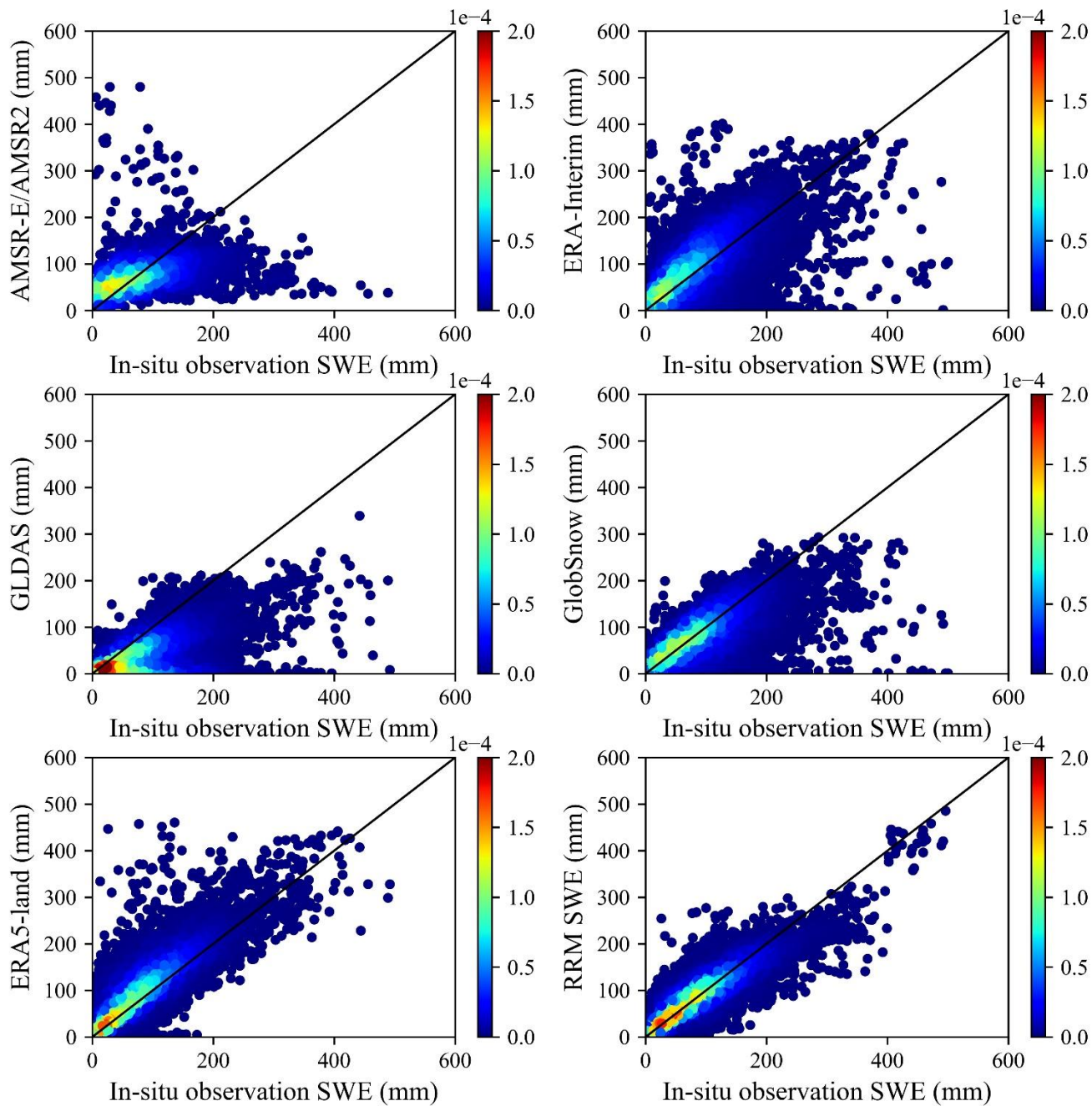
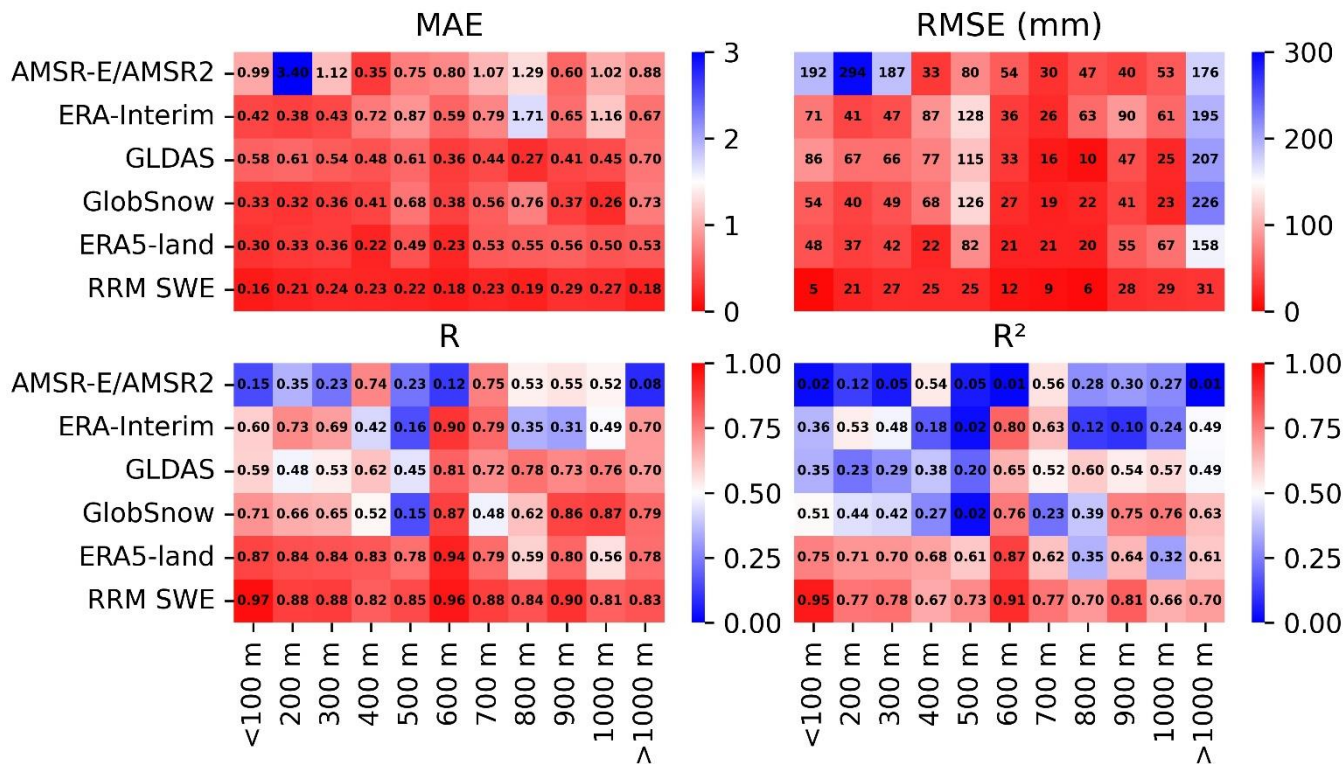


Figure 3: Accuracy comparison of various SWE products. The upper left sector represents the MAE, the upper right sector represents the RMSE, the lower left sector represents R, and the lower right sector represents R<sup>2</sup>. The sector axis represents the size of the error, and the color represents different SWE datasets.



534

535 **Figure 4:** Error verification density diagram (a total of 38807 sample points were used for verification). The color bar represents  
 536 the value of kernel density estimation. The closer the high-density area is to the 1:1 line, the higher the verification accuracy of the  
 537 dataset is at most of the measuring stations.



538

539

Figure 5: Comparison of the error between the RRM SWE and AMSR-E/AMSR2 SWE, ERA-Interim SWE, GLDAS SWE, GlobSnow SWE, and ERA5-land SWE at different altitudes (the abscissa represents the altitude gradient, and the ordinate represents different SWE datasets). The color bar indicates the error in each SWE dataset. The closer to red the color is, the higher the accuracy is. MAE: mean absolute error, RMSE: root mean square error, R: Pearson's correlation coefficient, R<sup>2</sup>: coefficient of determination).

544

545

546

547

548

549

550

551

552

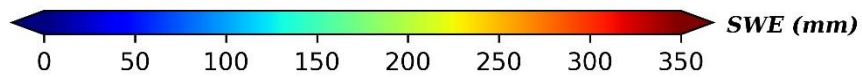
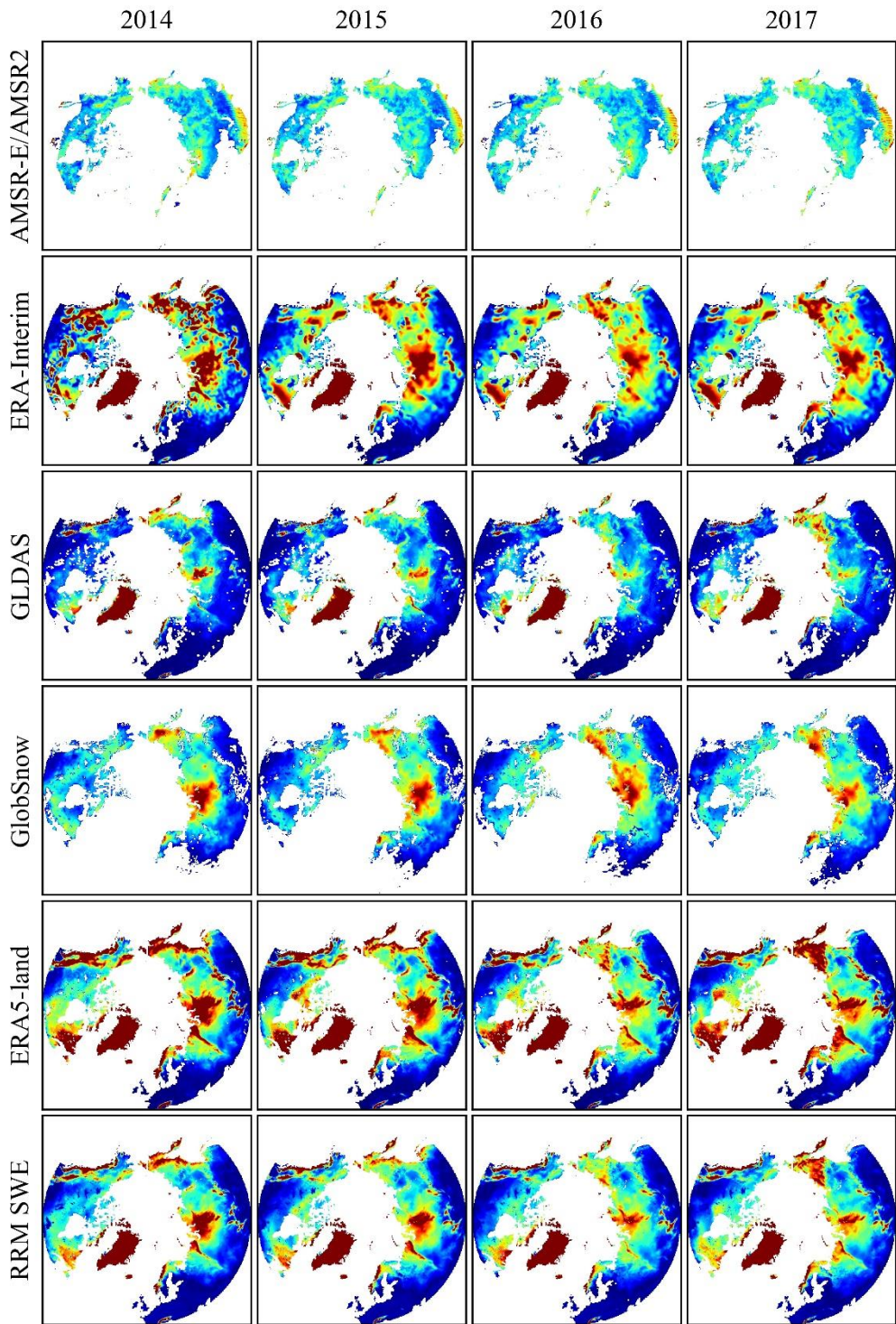
553

554

555 **Table 3: Error list for the station data and RRM SWE product in different regions.**

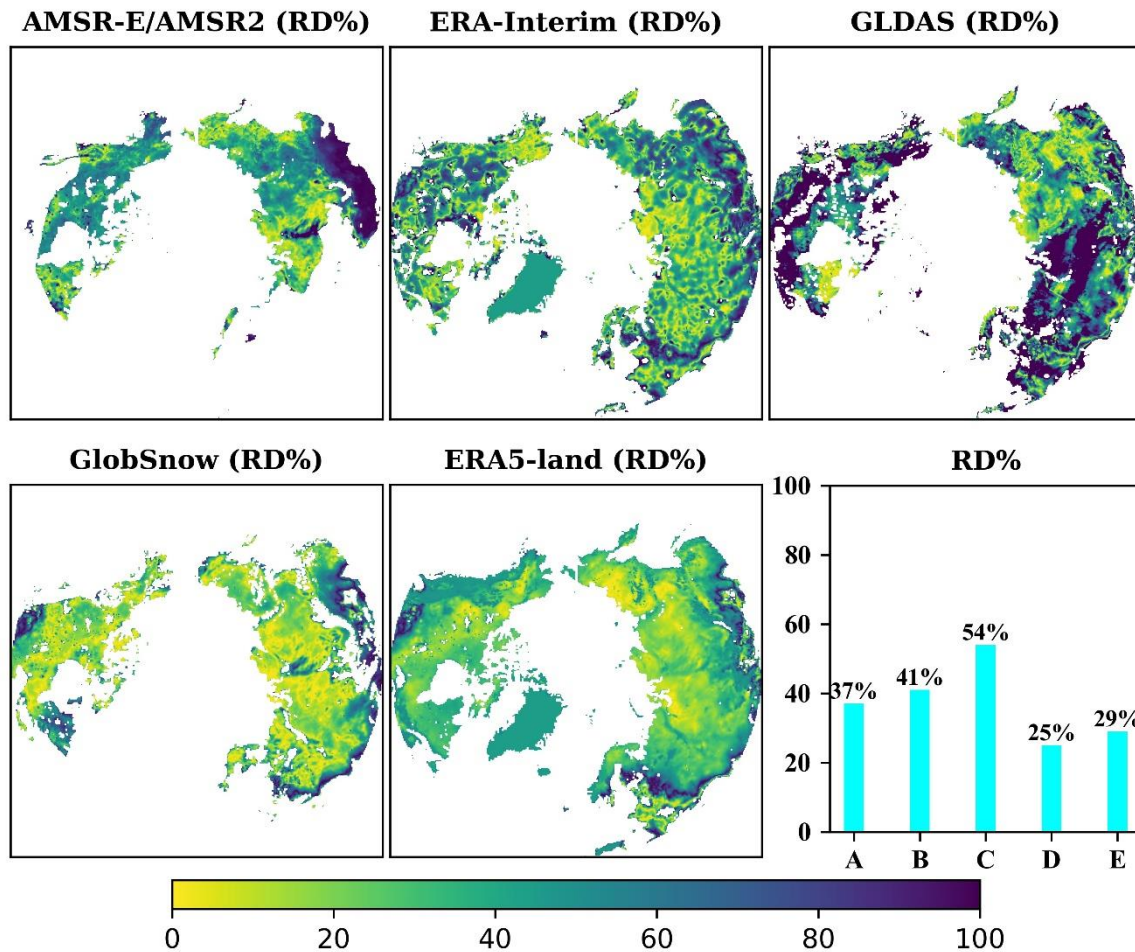
<b>Region</b>	<b>MAE</b>	<b>RMSE (mm)</b>	<b>R</b>	<b>R<sup>2</sup></b>
Russia	0.20	26.39	0.89	0.79
Canada	0.23	29.31	0.87	0.76
Finland	0.21	25.29	0.89	0.79

556



558 **Figure 6: Comparison of the spatial distribution characteristics between the RRM SWE and AMSR-E/AMSR2 SWE, ERA-**  
559 **Interim SWE, GLDAS SWE, GlobSnow SWE, and ERA5-land SWE (the four columns of images represent the comparison results**  
560 **in 2014, 2015, 2016, and 2017, respectively).**  
561





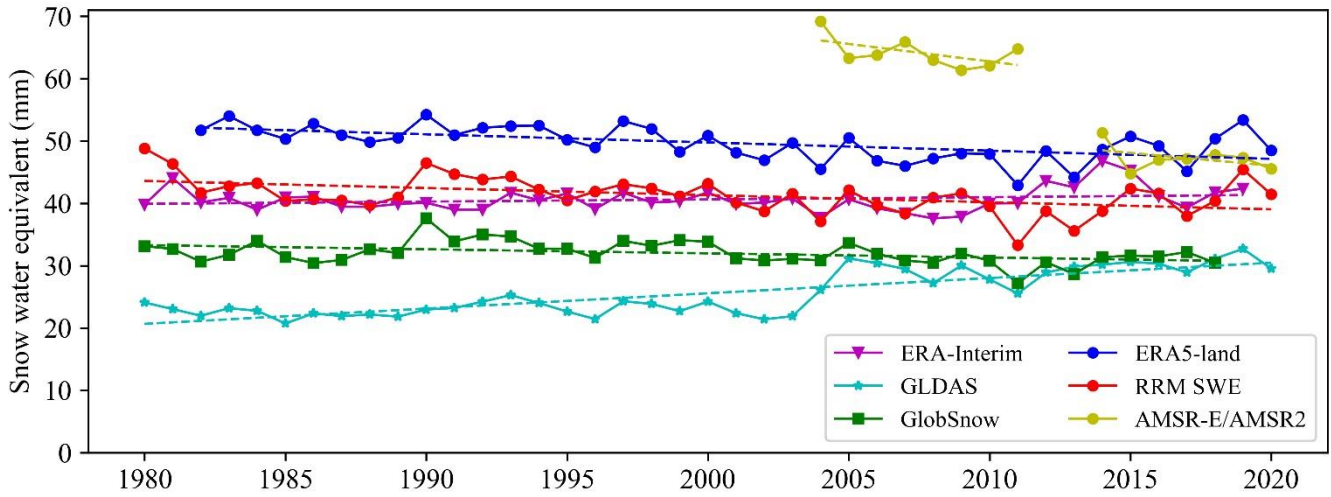
562

563 Figure 7: Temporal and spatial distributions of relative differences (RD%) between the RRM SWE and AMSR-E/AMSR2 SWE,

564 ERA-Interim SWE, GLDAS SWE, GlobSnow SWE, and ERA5-land SWE. Lower-right subgraph: Comparison of annual average

565 relative differences between the RRM SWE and AMSR2 SWE (A), ERA-Interim SWE (B), GLDAS SWE (C), GlobSnow SWE

566 (D), and ERA5-land SWE (E).



567

568

**Figure 8: Annual variation tendency in the AMSR-E/AMSR2 SWE, ERA-Interim SWE, GLDAS SWE, GlobSnow SWE, ERA5-land SWE and RRM SWE products from 1979 to 2019 (the dotted line is the trend line calculated based on the Mann-Kendall method).**

569

570

571

**Table 4: Results of the Mann-Kendall trend test performed for various snow water equivalent products from 1979 to 2019.**

<b>Data</b>	<b>P value</b>	<b>Test value</b>	<b>Trend</b>
AMSR-E/AMSR2	0.00	-3.26	Decreasing
ERA-Interim	0.27	1.08	No trend
GLDAS	7.29e-07	4.95	Increasing
GlobSnow	0.01	-2.54	Decreasing
ERA5-land	0.00	-3.43	Decreasing
RRM SWE	0.00	-3.00	Decreasing

\*Significance level  $\alpha = 0.05$